Metabolic Photofragmentation Kinetics for a Minimal Protocell: Rate-Limiting Factors, Efficiency, and Implications for Evolution

Chad Knutson**
Los Alamos National Laboratory

Gil Benkö†
Leipzig University

Tristan Rocheleau‡
University of California
at Santa Barbara

Fouzi Mouffouk§,¶
Argonne National Laboratory
Rush University

Jerzy Maselko#
University of Alaska at Anchorage

Liaohai Chen§,¶
Argonne National Laboratory
Rush University

Andrew P. Shreve††
Los Alamos National Laboratory

Steen Rasmussen*,‡‡,§§,¶¶,##
University of Southern Denmark
Los Alamos National Laboratory
Santa Fe Institute
University of Copenhagen

Abstract A key requirement of an autonomous self-replicating molecular machine, a protocell, is the ability to digest resources and turn them into building blocks. Thus a protocell needs a set of metabolic processes fueled by external free energy in the form of available chemical redox potential or light. We introduce and investigate a minimal photodriven metabolic system, which is based on photofragmentation of resource molecules catalyzed by genetic molecules. We represent and analyze the full metabolic set of reaction-kinetic equations and, through a set of approximations, simplify the reaction kinetics so that analytical expressions can be obtained for the building block production. The analytical approximations are compared with the full equation set and with corresponding experimental results to the extent they are available. It should be noted, however, that the proposed metabolic system has not been experimentally implemented, so this investigation is conducted to obtain a deeper understanding of its dynamics and perhaps to anticipate its limitations. We demonstrate that this type of minimal photodriven metabolic scheme is typically rate-limited by the front-end photoexcitation process, while its yield is determined by the genetic catalysis. We further predict that gene-catalyzed metabolic reactions can undergo evolutionary selection only for certain combinations of the involved reaction rates due to their intricate interactions. We finally discuss how the expected range of metabolic rates likely affects other key protocellular processes such as container growth and division as well as gene replication.

Keywords
Metabolism, photofragmentation, kinetics, gene selection, protocell

* Corresponding author.
** EES-2, Los Alamos National Laboratory, MS-D462, Los Alamos, NM 87545. E-mail: knutson@lanl.gov
† Graduiertenkolleg Wissensrepräsentation, Leipzig University, Leipzig, Germany. E-mail: gil@bioinf.uni-leipzig.de
‡ University of California at Santa Barbara, Santa Barbara, CA 93106. E-mail: tristanr@lanl.gov
§ Argonne National Laboratory, Argonne, IL 60439. E-mail: Fouzi_Mouffouk@rush.edu (F.M.); lhchen@anl.gov (L.C.)
¶ Rush University, Chicago, IL 60612.
# University of Alaska at Anchorage, Anchorage, AK 99508. E-mail: afjml@uaa.alaska.edu
†† MPA-CINT, Los Alamos National Laboratory, MS-K771, Los Alamos, NM 87545. E-mail: shreve@lanl.gov
‡‡ Center for Fundamental Living Technology (FLinT), Department of Physics and Chemistry, University of Southern Denmark, DK-5230 Odense, Denmark. E-mail: steen@ifk.sdu.dk
§§ Self-Organizing Systems (SOS), EES-6, Los Alamos National Laboratory, MS-D462, Los Alamos, NM 87545.
¶¶ Santa Fe Institute, Santa Fe, NM 87501.
University of Copenhagen, IMBG, Blegdamsvej 3, DK-2200, Denmark.

I Introduction

The importance of studying minimal protocells [9, 19, 26] lies, among other things, in furthering an understanding of what life is and the fundamental phenomena associated with life. A minimal protocell may consist of three component molecules: lipids for the container; precursor and energy-capture molecules for the metabolic processes; and information molecules (genes) for the genetic material, as outlined in [20]. In this work we investigate the reaction kinetics of a simple metabolic system that could operate as part of such a protocell. The metabolic scheme uses light energy to drive a reaction that produces additional molecules for the information molecules and for the container. The novel feature of this scheme is that the protocell's information molecules are directly involved in the metabolic processes.

The use of light energy to drive chemical reactions is expanding to more complex systems. Photochemistry is currently used in applications such as photolithography and X-ray crystallography to generate the desired product in a controllable manner, enabling the production of nanometer-scale images. Much work in the area of artificial photosynthesis is ongoing, and some promising advancements have occurred, including the generation of a protonmotive force across a membrane by embedding a photosensitizer within the membrane [13, 25]. Further breakthroughs could lead to functioning photodriven metabolic systems for artificial cells.

Over the last few decades, a considerable amount of knowledge has been accumulated on electron transfer processes initiated by photoexcitation of potential donors or acceptors that typically show no interaction in their ground states. The intermediates, generated from single-electron-transfer quenching of the excited state of donor or acceptor, can provide useful chemical reactions [1, 6, 27]. An area of growing interest is radical-ion fragmentation initiated by photoinduced electron transfer [7, 17, 18, 28]. Several of these reactions are very clean processes in which a single carbon-carbon, carbon-oxygen, or carbon-nitrogen bond is selectively broken in high chemical yield and sometimes with reasonable quantum yield. In general, the quantum efficiency of these reactions depends on the competition of three processes after quenching the excited state through the electron transfer: back electron transfer (k_{back}), radical-ion pair separation (k_e), and bond cleavage (k_L) as outlined in Figure 1.

Despite the discovery of several systems that undergo efficient bond cleavage, the quantum efficiency of the reaction is generally small. The relatively fast return electron transfer within the geminate radical-ion pair and the slow bond fragmentation rate are the primary causes of poor quantum efficiency. When the rate of fragmentation (k_L) is much lower than the rates of back electron transfer (k_{back}) and ion pair separation (k_e) (which is true for most cases), the reaction quantum yield largely depends on the ratio of k_e to k_{back}, because deactivation of the separated radical ions through second-order recombination is a slow process, especially when conventional light sources are used. Otherwise, higher quantum efficiency can be obtained if k_L is comparable to or larger than k_{back} (or k_e). It is quite common to encounter k_{back} of 10^{10} s^{-1} and higher, which results in quantum yields of

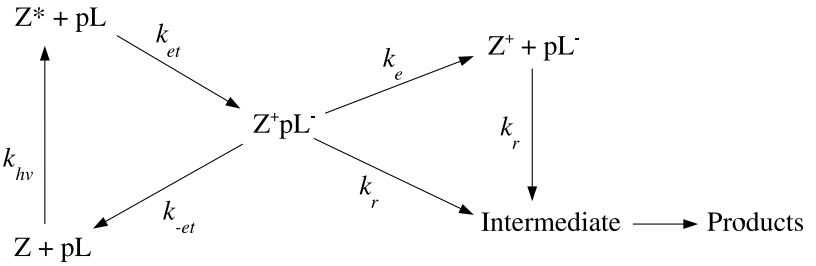

Figure I. General scheme of the initial processes for photoinduced electron transfer (PET) fragmentation reactions. A photosensitizer Z is initially excited by light, causing a charge separation and a transfer of an energy-rich electron to a reactant molecule pL, which eventually undergoes a fragmentation reaction to form new products.

separated radical ion of 5% to 10% or less. In order to improve the quantum efficiency of a bond cleavage reaction, one can increase either k_e or k_L. However, in most solvents, k_e seems to be rather insensitive (ca. 5×10^8 to 10^9 s^{-1}) to the structure of the radical-ion pair or to the reaction energetics. Using an electron relay system for an efficient k_L is the most commonly used method to increase reaction quantum efficiency.

Recently, bio-related molecules that may be used as information molecules, such as peptide, DNA, or peptide nucleic acid (PNA), have been demonstrated to be excellent electron relay systems [2, 5, 10, 11, 15, 21]. Since the efficiency of charge transfer is sequence-dependent, we can use certain sequences of DNA or PNA strands as an electron relay system to control the fragmentation reaction efficiency. This enables an avenue to couple the gene information to the production of lipid molecules. Rationally designed sequences could generate the radical ion of the other reactant at a much higher quantum yield, which would subsequently undergo fragmentation to form lipid molecules. This might produce a selection pressure to drive protocell evolution toward PNA sequences with optimal electron transfer rates.

It has been well established that phenacyl esters can undergo photoinduced C–O bond scission to form acetophenone ($PhCOCH_3$) and the corresponding carboxylic acid (RCO_2H, surfactant) in the presence of appropriate electron donor molecules [3]. However, the quantum efficiency is very low (ca. 0.01–0.05) because of fast back electron transfer. As mentioned earlier, a sensitizer coupled with an electron relay system can be introduced to block back electron transfer, increasing the quantum yield of the reaction. A direct autocatalytic feedback between PNA proto-genes and the production of both lipid molecules and more PNA precursor molecules can be implemented by using PNA modified by a donor sensitizer (Z) as the electron relay system to photofragment various phenacyl esters ($PhCOCH_2$–OCOR, where R is a long carbon chain). The excited state of the sensitizer reduces phenacyl esters, and then the sensitizer cation radical is reduced by PNA molecules. Stilbene derivatives appear to be suitable sensitizers for this process.

The objective of this article is to introduce a minimal photochemical system that can be used as the metabolic system of a protocell. A key feature of this system is that a genetic molecule is directly involved (or must be present in order for the system to function correctly). The desired end product of the process is a fatty acid molecule for the protocell aggregate and/or PNA oligomers that can undergo template-directed polymerization. The kinetics of the photochemical system are investigated, and the resulting equations are simplified to obtain analytical expressions for the overall metabolic production rate. The consequences of a catalytic coupling between a metabolic container production and gene replication are discussed in [16, 22].

2 The Metabolic Reactions

In the proposed protocell model, first-generation protocells are formed by self-assembly [20]. The lipids that form the protocell container are carboxylic acids (L), which form micellar structures at appropriate concentrations, pH values, and salt concentrations. The hydrophobic photosensitizers (Z) (either stilbenes or aromatic amines) are present within the oily interior of the micelle. The genes are modified PNA chains that partition to the interface of the container and the surrounding solution. However, the genes could be any amphiphilic or hydrophilic nucleic acid molecule that associates with lipid aggregates. The resource molecules consist of precursor lipids (pL) (e.g., phenacyl) and precursor information molecules (pO) that must be continuously added to the solution. These resource molecules are either hydrophobic or amphiphilic, so they partition to the container interior or surface. The metabolic system transforms precursor lipids (pL) into lipids (L), the container building blocks, and transforms amphiphilic precursor PNA oligomers (pO) into functional oligomers that can ligate (polymerize). The pOs attach to the aggregate surface with the hydrophobic backbone anchored into the interior.

All electron transfer reactions are assumed to occur within the aggregate's oily phase or interface, because the double-stranded PNA and the photosensitizer are immersed in the lipid aggregate or are

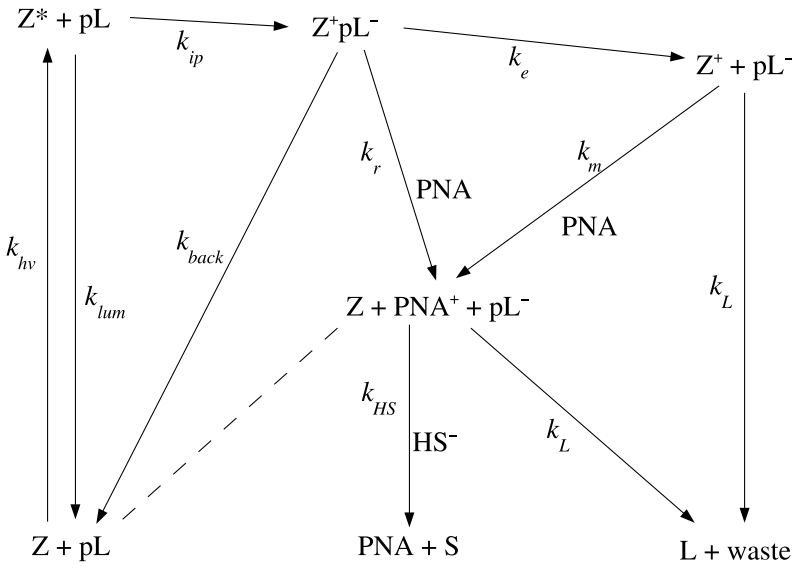

Figure 2. Reaction diagram showing reaction rates and the reactions between precursor lipids (pL), sensitizers (Z), catalytic information molecules (PNA), and lipids (L).

deeply anchored at the interface. We can assume either that the hydrophobic photosensitizer (Z) is covalently bonded to the PNA backbone, increasing its hydrophobicity, or that it exists in sufficient concentration within the aggregate.

The metabolic scheme for the protocell is presented in Figure 2. Upon irradiation with light of an appropriate wavelength, the sensitizer is excited (Z^*) with rate constant $k_{h\nu}$, and due to the close proximity to the precursor lipids (pL) or precursor oligomers (pO), this causes a charge separation, and thus a contact ion pair, leaving the sensitizer positively charged (Z^+) and the nearby precursor molecules (pL^- or pO^-) negatively charged (rate k_{ip}). For most excitations, the charges will quickly rejoin, dissipating the energy by emission and returning the system to the ground state (rate constant k_{back}). This back reaction inhibits any significant quantum yield from the photochemical reaction.

However, double stranded PNA with an appropriate base composition and sequence [presumably two neighboring guanine (G) bases] should be able to act as a catalyst for the reaction through an electron relay system [14, 20]. Guanine bases within the PNA string can reduce Z^+ by charge transfer ($G \rightarrow G^+ + e^-$) with rate constant k_r. The positively charged PNA may be neutralized by HS^- or some other terminal electron donor (rate constant k_{HS}). This process separates the charges and allows the energized and negatively charged precursor molecule (pL^- or pO^-) sufficient time to undergo a fragmentation process through the breakage of the ester bond, resulting in the production of a functional oligomer or lipid molecule.

Another possibility for the Z^+pL^- contact ion pair is that the cation and anion may separate (rate constant k_e). This is problematic because Z^+ may then be reduced by a number of different molecules present in solution, including water, instead of the information molecule (rate constant k_m). Along this pathway, the information molecule is not functionally part of the metabolic scheme, and the necessary gene control of the system breaks down.

We can now write the reaction-kinetic reactions for lipid production within the photometabolic system. The production of functional PNA oligomers follows the same pattern. We assume that the PNA gene concentration in the aggregates is constant and that the ratio between single- and double-stranded PNA within the aggregates is fixed:

$$\frac{d[\mathrm{pL}]}{dt} = -k_{\mathrm{ip}}[Z^*][\mathrm{pL}] + k_{\mathrm{back}}[Z^+\mathrm{pL}^-], \tag{1}$$

$$\frac{d[\mathrm{Z}]}{dt} = -k_{h\nu}[\mathrm{Z}] + k_{\mathrm{lum}}[\mathrm{Z}^*] + k_{\mathrm{back}}[\mathrm{Z}^+\mathrm{pL}^-] + (k_r[\mathrm{Z}^+\mathrm{pL}^-] + k_m[\mathrm{Z}^+])[\mathrm{PNA}], \tag{2}$$

$$\frac{d[\mathrm{Z}^*]}{dt} = k_{h\nu}[\mathrm{Z}] - k_{\mathrm{lum}}[\mathrm{Z}^*] - k_{\mathrm{ip}}[\mathrm{Z}^*][\mathrm{pL}], \tag{3}$$

$$\frac{d[\mathrm{Z}^+\mathrm{pL}^-]}{dt} = k_{\mathrm{ip}}[\mathrm{Z}^*][\mathrm{pL}] - k_{\mathrm{back}}[\mathrm{Z}^+\mathrm{pL}^-] - k_e[\mathrm{Z}^+\mathrm{pL}^-] - k_r[\mathrm{Z}^+\mathrm{pL}^-][\mathrm{PNA}], \tag{4}$$

$$\frac{d[\mathrm{Z}^+]}{dt} = k_e[\mathrm{Z}^+\mathrm{pL}^-] - k_m[\mathrm{Z}^+][\mathrm{PNA}], \tag{5}$$

$$\frac{d[\mathrm{pL}^-]}{dt} = k_e[\mathrm{Z}^+\mathrm{pL}^-] + k_r[\mathrm{Z}^+\mathrm{pL}^-][\mathrm{PNA}] - k_L[\mathrm{pL}^-], \tag{6}$$

$$\frac{d[\mathrm{L}]}{dt} = k_L[\mathrm{pL}^-]. \tag{7}$$

Values for the rate constants used in this work are shown in Table 1. Values for rate constants that could not be found in the literature are obtained by fitting fatty acid production rates from Sundararajan and Falvey [24] using known literature values where possible. The photoexcitation rate may change significantly for different light sources or sensitizer molecules. Insufficient charge transfer studies have been performed with PNA compared with DNA, so we estimate $k_r \approx 10^9\ (\mathrm{M\ s})^{-1}$, as is the case in DNA [4]. Experiments are underway to identify how the fragmentation kinetics depends on the PNA sequence.

Table 1. Estimated values of rate constants. * indicates that values have been estimated by fitting fatty acid production rates from Sundararajan and Falvey [24].

Parameter	Value	Units	Reference
$k_{h\nu}$	10^0	s^{-1}	*
k_{lum}	10^8	s^{-1}	*
k_{ip}	3×10^9	$(M\ s)^{-1}$	[23, 24]
k_{back}	10^4	s^{-1}	[12, 23]
k_r	10^9	$(M\ s)^{-1}$	[4]
k_e	10^6	s^{-1}	[12]
k_m	10^6	$(M\ s)^{-1}$	[4]
k_L	10^6	s^{-1}	*

Overall, the values presented for the parameters in Table 1 are thus constrained by experimental studies or physical reasonableness. However, in most instances these should be considered as order-of-magnitude estimates. A more precise determination of any one parameter is difficult because systematic experimental studies to measure each of these parameters are still lacking. However, the large uncertainties in value of any individual parameter do not influence our primary conclusions, provided that, as seems quite likely, the excitation rate of the photosensitizer remains the overall rate-limiting step.

3 Separation of Reaction Time Scales

The objective of the following analysis is to obtain expressions for the rates of formation of L and of removal of pL that depend only on the pL concentration and the rate constants. The first step of the scheme that involves pL is a bimolecular reaction with Z^*. The concentration of Z^* changes with time in the scheme, but a reasonable estimate may be obtained by assuming that the concentrations of all species containing the sensitizer reach equilibrium before significant changes in pL are observed. Additionally, we assume that $k_r[\mathrm{PNA}] \gg k_e$, so that the concentration of Z^+ may be set equal to zero. Mathematically, the time rates of change for species Z, Z^*, and Z^+pL^- are set equal to zero. These equations are solved simultaneously along with the mass balance of the sensitizer ($[Z] + [Z^*] + [Z^+pL^-] = Z_0$). The value of $[Z^*]$ is estimated as

$$[Z^*]_{\mathrm{eq}} \approx \frac{k_{h\nu}(k_{\mathrm{back}} + k_r[\mathrm{PNA}])Z_0}{k_{h\nu}k_{\mathrm{ip}}[\mathrm{pL}] + (k_{\mathrm{back}} + k_r[\mathrm{PNA}])(k_{\mathrm{ip}}[\mathrm{pL}] + k_{\mathrm{lum}} + k_{h\nu})}. \tag{8}$$

This approximation may be simplified when terms differ by orders of magnitude or more.

To contract the remaining steps of the reaction scheme, we employ the approximations described in the Appendix. The next section of the metabolic process converts pL to pL^-. This set of reactions has the same form as the reaction scheme in Equation 18. The first forward reaction is the bimolecular reactions between pL and Z^* to form the contact ion pair Z^+pL^-. The contact ion pair may proceed in the forward direction by two different pathways, but we have already assumed that $k_r[\mathrm{PNA}] \gg k_e$, so only the electron transfer from PNA needs to be considered. Alternatively, the contact ion pair may undergo back electron transfer to the ground state. The rate equation for converting pL to pL^- can be approximated by

$$\frac{d[\mathrm{pL}]}{dt} \approx -k_{\mathrm{first}}[\mathrm{pL}], \tag{9}$$

where

$$k_{\mathrm{first}} = \frac{[Z^*]_{\mathrm{eq}}k_{\mathrm{ip}}k_r[\mathrm{PNA}]}{[Z^*]_{\mathrm{eq}}k_{\mathrm{ip}} + k_{\mathrm{back}} + k_r[\mathrm{PNA}]}. \tag{10}$$

The back reaction in this equation is slightly different from the reaction scheme in Equation 18 because the sensitizer in Z^+pL^- returns to the ground state rather than to the excited state. But this may be neglected because the sensitizer species are assumed to be in equilibrium.

The final step that we consider is the fragmentation of pL^- to produce lipids. If Equation 9 is taken as the rate for a single reaction step, then a combined rate for this step and the fragmentation

reaction may be obtained using the reaction in Equation 16. Thus, the overall rate of lipid production is given by

$$k_{\text{tot}} \approx \frac{k_{\text{first}} k_L}{k_{\text{first}} + k_L}. \tag{11}$$

Thus, the rate of change of pL and L may be estimated by

$$\frac{d[\text{pL}]}{dt} \approx -k_{\text{tot}}[\text{pL}] \tag{12}$$

$$\frac{d[\text{L}]}{dt} \approx k_{\text{tot}}[\text{pL}]. \tag{13}$$

These equations are easily solved using the initial conditions that $[\text{pL}](t = 0) = \text{pL}_0$ and $[\text{L}](t = 0) = 0$.

We consider two limiting cases for lipid production that depend on the value of photoexcitation rate, $k_{h\nu}$. Because the concentration of PNA is very small (10^{-4} M), the electron transfer from PNA to the sensitizer controls the overall rate of reaction once a sensitizer is excited. In both fast and slow excitation, the overall rate constant may be approximated as $k_{\text{tot}} \approx [Z^*]_{\text{eq}} k_{\text{ip}}$, where the concentration of Z^*_{eq} depends on the excitation rate. For fast excitation, $[Z^*]_{\text{eq}} \approx k_r[\text{PNA}]Z_0/(k_{\text{ip}}[\text{pL}])$. Then, the rate of change for L concentration is simply given by

$$\frac{d[\text{L}]}{dt} \approx k_r[\text{PNA}]Z_0, \tag{14}$$

so that the removal rate of pL is constant as long as sufficient pL is present.

For slow photoexcitation, the rate-limiting step is the photoexcitation of the sensitizer molecule. In this case, the rate equations for pL and L are Equations 12 and 13, respectively, and the rate equation for L is given by

$$\frac{d[\text{L}]}{dt} \approx \frac{k_{h\nu}}{k_{\text{lum}}} k_{\text{ip}} Z_0[\text{pL}]. \tag{15}$$

In this case, production of L is exponential with time.

In Figure 3, concentrations of precursors and lipids are plotted versus time for both both fast and slow photoexcitation rates. In each case, both the simplified equations and numerical solutions to the full set of equations are plotted. Contact ion pair separation is included in these calculations with the value of k_e set equal to the value shown in Table 1. Excellent agreement is achieved for lipid formation in each case.

4 Rate Limitations and Electron Transfer Efficiency

For the estimated values of reaction rate constants in this study, the rate-limiting step is the photoexcitation of the sensitizer. The low excitation rate results from using a typical (visible light) lamp to generate photons. The excitation rate may be increased by several orders of magnitude by using lasers of appropriate wavelength. Thus, we expect that a wide range of values is possible for $k_{h\nu}$.

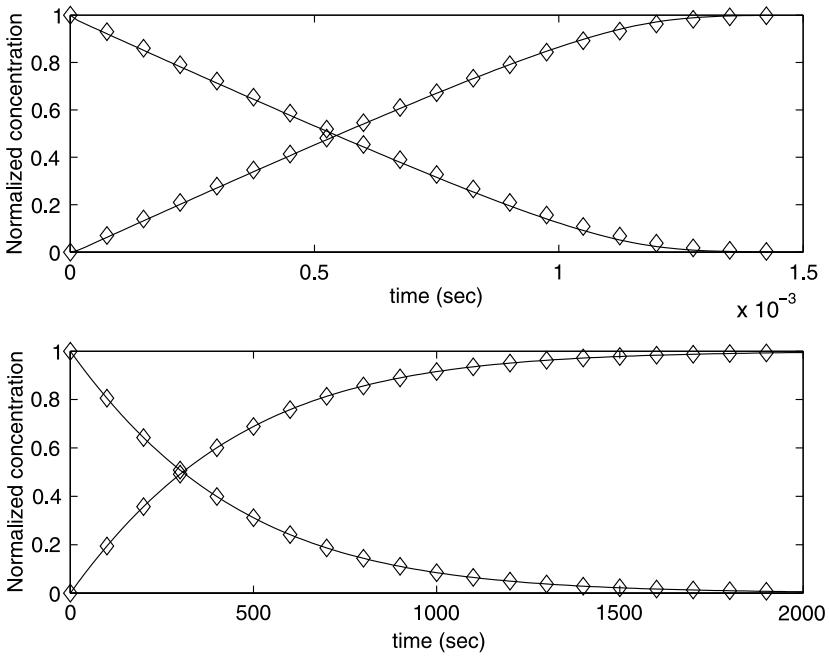

Figure 3. Concentrations of lipids and precursor lipids for fast (upper) and slow (lower) photoexcitation. Numerical simulations of the full reaction system (solid lines) are compared with the analytical solution of the simplified equations (dashed). Curves starting at concentration equal to one correspond to pL, and curves starting at concentration equal to zero correspond to L. For each case, $pL_0 = 0.01$ M, $Z_0 = 0.0001$ M, [PNA] = 0.0001 M, $k_{lum} = 10^8$ s^{-1}, $k_{ip} = 3 \times 10^9$ (M s)$^{-1}$, $k_{back} = 10^4$ s^{-1}, $k_r = k_m = 10^9$ (M s)$^{-1}$, and $k_L = 10^5$ s^{-1}. The value of $k_{h\nu}$ is 10^7 s^{-1} for fast excitation and 10^0 s^{-1} for slow excitation.

In Figure 4, the half-life of lipid precursors is determined for a range of values for $k_{h\nu}$. Results are obtained by numerically solving the full set of differential equations (Equations 1–7) to determine the time at which half of the initial lipid precursors have been converted to lipids. For values of $k_{h\nu}$ less than 10^6 s^{-1}, the photoexcitation step is the rate-limiting step of the overall reaction, as demonstrated by

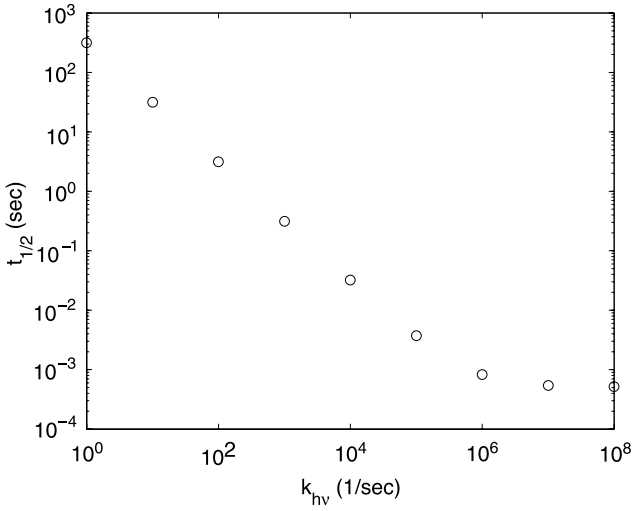

Figure 4. Time to transform one-half of pL to L for a range of $k_{h\nu}$ (photoexcitation rate) values. Default values are used for other parameters as well as initial concentrations of each species, and the graphs are generated from simulating the full reaction kinetic system. Note that for $k_{h\nu} > 10^6$ s^{-1} the rate-limiting step in the metabolic system is no longer photoexcitation. For $k_{h\nu} < 10^6$ s^{-1} photoexcitation is the rate-limiting step.

the linear dependence of the lipid precursor half-life on the value of $k_{h\nu}$. For values of $k_{h\nu}$ greater than 10^6 s^{-1}, the overall rate becomes independent of the value of $k_{h\nu}$ and the time scale of the reaction approaches 10 μs. However, the theoretical maximum excitation rate is on the order of 10^8 s^{-1}, with the greatest practical rate closer to 10^6 s^{-1}. Thus, for all practical cases, the rate-limiting step in the reaction scheme is photoexcitation.

The rate of lipid (and oligomer) production depends greatly on the relative rates of forward and backward reactions. In the proposed scheme, there are two steps in which forward and backward reactions must compete. The first step involves the competition between electron transfer from the excited sensitizer to the precursor and luminescence of the photosensitizer. The relative rates of these steps are largely dependent upon the sensitizer used and the precursor and sensitizer concentrations. The second step, which is less understood, is the competition between back electron transfer within the contact ion pair (Z^+pL^-) and electron transfer from PNA to the contact ion pair. In bulk solution, concentrations of sensitizers and PNA tend to be on the order of millimolar, so the binary reaction rate is slow. However, because the sensitizers and PNA accumulate at the protocell containers, the local concentrations within the protocells can be greatly enhanced. The probability of the forward reaction occurring may also be increased by covalently linking the PNA template molecules to the sensitizers.

5 PNA Selectivity and Evolution

In order for protocell evolution to occur, a selective pressure must exist. It is hypothesized that the electron transfer rate from PNA molecules to sensitizers depends on the base sequence of PNA, so that protocells with optimal sequences have better metabolisms and will eventually become dominant. However, for most of the estimated rates in this investigation, the electron transfer rate from PNA is very fast compared to the photoexcitation rate. This means that the selective pressure for all

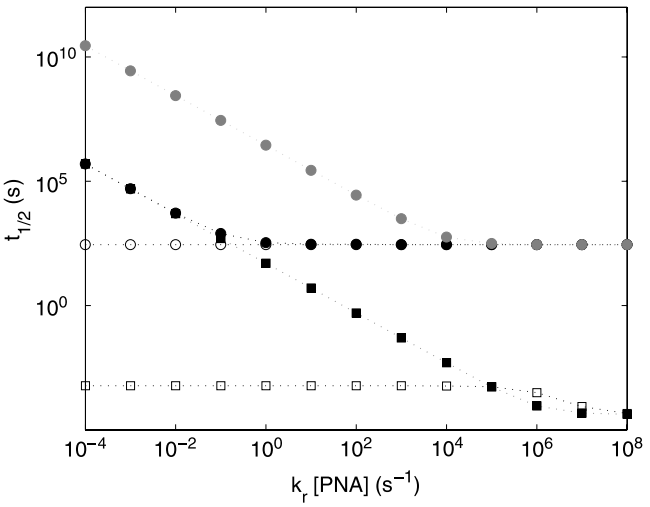

Figure 5. Time to transform one-half of pL to L for a range of values for k_r[PNA]. Results for both fast (squares) and slow (circles) excitation are shown. Three cases are shown: (i) k_m[PNA] = 10^5 s^{-1} and k_e = 10^6 s^{-1} (open symbols), (ii) k_r[PNA] = k_m[PNA] and k_e = 10^6 s^{-1} (black symbols), and (iii) k_e = 0 (gray symbols). Curves are generated by simulating the full reaction-kinetic system with standard parameters. Note that for the more realistic case with slow excitation rate (circles), no selection is possible even for very small values of k_r[PNA] in case (i). No gene selection is possible for k_r[PNA] > 10^{-1} s^{-1} in case (ii) and for k_r[PNA] > 10^4 s^{-1} in case (iii). Selection, and thus evolution, are possible between genes with different k_r[PNA] values below these values or between different sequences with k_r[PNA] values below and above these values, respectively. However, the catalytic PNA is further modulated by the balance between the k_r[PNA] and k_e pathways, as well as the background reactions. See text for discussion.

sequences with electron transfer rates faster than the photoexcitation step will be the same because the overall metabolic rate is unaffected by the rate of the gene catalyzed step.

In Figure 5, the time scale for lipid production is shown for varying rates k_r[PNA] of electron transfer from PNA using both fast (10^7 s^{-1}) and slow (10^0 s^{-1}) photoexcitation rates based on the full reaction kinetic system given by Equations 1–7. In this exploration three cases are discussed: (i) k_m[PNA] $= 10^5$ s^{-1} and $k_e = 10^6$ s^{-1}, (ii) k_r[PNA] $= k_m$[PNA] and $k_e = 10^6$ s^{-1}, and (iii) $k_e = 0$. In case (iii), the value of k_m[PNA] is irrelevant because the reaction cannot proceed along this pathway.

For fast photoexcitation rates in case (i), small values of k_r[PNA] do not affect the lipid production, because the reaction proceeds along the $k_e = 10^6$ s^{-1} pathway of the scheme. However, as the relative values between these rates differ in favor of the k_e pathway, the catalytic PNA control of lipid production also vanishes, since the charge recombination between the separated contact ions Z^+ and pL^- can be ignored for all practical purposes in this situation. This means that the lipid precursor fragmentation of the pL^- ion occurs independently of any possible PNA catalytic reduction of the Z^+ ion.

In case (ii) where the k_r[PNA] values are small enough, the rate-limiting step of lipid production is again electron transfer from PNA both for the fast and the slow photoexcitation. As expected, the PNA catalytic range is much larger for the fast photoexcitation, as the PNA catalysis starts to become the rate-limiting step already for k_r[PNA] $< 10^6$ s^{-1}. For the slow excitation process k_r[PNA] $< 10^0$ s^{-1} becomes rate-limiting. Again, $k_e < k_r$[PNA] is necessary to ensure that a majority of the reaction proceeds down the k_r[PNA] pathway to maintain the catalytic PNA control of the lipid production.

For case (iii) the catalytic PNA lipid production pathway is preserved for all values. No difference is observed between this case and the previous one for the fast excitation rate. However, for the slow excitation rate, a significant difference is observed as k_r[PNA] decreases. This is because the back electron transfer pathway becomes dominant. As expected, the curve breaks off for k_r[PNA] $< k_{back} = 10^4$ s^{-1}.

So when is PNA gene selection possible in this simple metabolic scheme? Since photoexcitation is expected to be slow, the effective catalytic effect of different PNA sequences may be difficult to observe unless the sequences have significantly different charge transfer rates. In order to observe changes in the lipid production rate for two different PNA base sequences, the value of k_r[PNA] for at least one of the sequences must be less than 1 s^{-1} in case (ii) and less than 10^4 s^{-1} in case (iii). If either of these conditions is not satisfied, the lipid production rates will be independent of the PNA base sequences, and evolution towards protocells with optimal PNA base sequences may not occur. See Figure 5 for further discussion.

Finally it should be noted that a background charge transfer rate is always present, which will tend to neutralize the ion pairs independently of all other reactions. This means that, in practice, slow PNA electron transfer rates may have vanishing catalytic effect due to these background reactions. The scale of the background is dependent on many factors, such as temperature, pH, salt concentration, and of course, the ion pair species involved.

6 Discussion and Conclusions

A successful metabolic system is a key step in the attempt to develop a viable protocell. The clear conclusions we can draw from our analysis are: (i) The rate-limiting step in the proposed metabolic scheme is the photoexcitation of the sensitizer. (ii) The metabolic yield is determined by the efficiency of the genetic catalysis of the forward fragmentation reaction compared to the back reaction. Without catalysis the overall process is dominated by the back reaction. (iii) Only for certain parameter combinations is catalytic gene selection possible, as the selection must be involved in a rate-limiting step. This means that the efficiency of the gene-catalyzed rates is affected both by the photoexcitation rate and by the rate at which the contact ion pairs separate.

The likely time scale of the metabolic production can now be considered in the context of the time scales of the other protocellular processes [22]. Obviously, the aggregate lifetime must be long enough to ensure container continuity both for the metabolic renewal process and for the inheritance through the template-directed replication time. However, the balance between the lipid aggregate relaxation time and the lipid production time can also be critical.

A visible-light-driven metabolism of the kind we have proposed here, with no use of lasers, has an overall conversion rate limited by the sensitizer photoexcitation step, which is of the order of magnitude of one metabolic conversion per sensitizer per second. If we assume an aggregate size of 100 lipids (a micelle) loaded with a similar set of precursors and the presence of a single photosensitizer, the lower bound on the metabolically determined protocellular generation time is 100 s, which is extremely fast compared to any contemporary organism. The lipid aggregate relaxation time is on the order of nanoseconds, and is therefore certainly less than microseconds [8]. Thus the aggregate will reach equilibrium much faster than the metabolic rate can drive it out of equilibrium.

The metabolic transformation of oil-like molecules to surfactant molecules drives the aggregate out of equilibrium. As this occurs, several processes come into play, and the balance among them is important for overall protocellular dynamics. The generated nonequilibrium state of the aggregate could destabilize it and cause the aggregate to split into two or more new aggregates. The path taken by the unstable aggregate to equilibrium depends on the metabolic conversion rate compared to the aggregate relaxation rate and on the aggregate composition. During conversion, an adiabatic exchange of lipid molecules with the background solution occurs simultaneously. In one extreme, very slow metabolic conversion could result in a continuous aggregate equilibrium where the aggregate continuously shrinks by ejecting excess lipids, preventing true aggregate division. In another extreme, very fast metabolic conversion could ensure an instant aggregate instability with subsequent division. Yet, another situation is possible, where moderate metabolic conversion modifies the relative oil-surfactant composition to a point where the aggregate eventually reaches a critical oil-lipid composition where it becomes unstable and splits. This last scenario is the most likely target for our protocell design, as a metabolic conversion rate that is significantly faster than the aggregate relaxation rate seems unrealistic in view of the analysis in this work.

Acknowledgments

We are grateful for input and constructive criticism received from James Bailey, James Boncella, Michael DeClue, Goran Goranovic, Pierre-Alain Monnard, William Woodruff, and Hans Ziock, as well as discussions with other team members on the Protocell Assembly (PAs) and Programmable Artificial Cell Evolution (PACE) projects. This work is in part supported by a Los Alamos National Laboratory (PAs) LDRD-DR grant and a grant from the European Commission's 6th Framework on emerging information technologies (PACE).

References

1. Albini, A., & Sulpizio, A. (1988). *Photoinduced electron transfer*. Amsterdam: Elsevier Science Publishers.
2. Armitage, B., Ly, D., Koch, T., Frydenlund, H., Orum, H., Batz, H. G., & Schuster, G. B. (1997). Peptide nucleic acid DNA duplexes: Long range hole migration from an internally linked anthraquinone. *Proceedings of the National Academy of Sciences of the U.S.A.*, *94*, 12320–12325.
3. Banerjee, A., & Falvey, D. E. (1997). Protecting groups that can be removed through photochemical electron transfer: Mechanistic and product studies on photosensitized release of carboxylates from phenacyl esters. *Journal of Organic Chemistry*, *62*, 6245–6251.
4. Barton, J. K. (1998). DNA-mediated electron transfer: Chemistry at a distance. *Pure & Applied Chemistry*, *70*, 873–879.
5. Burrows, C. J., & Muller, J. G. (1998). Oxidative nucleobase modifications leading to strand scission. *Chemical Reviews*, *98*, 1109–1151.
6. Chen, L., Farahat, M. S., Gan, H., Farid, S., & Whitten, D. G. (1995). Photoinduced electron transfer double fragmentation: An oxygen-mediated radical chain process in the cofragmentation of aminopinacol donors with organic halides. *Journal of the American Chemical Society*, *117*, 6398–6399.

7. Chen, L., Lucia, L., & Whitten, D. G. (1998). Cooperative electron transfer fragmentation reactions. Amplification of a photoreaction through a tandem chain fragmentation of acceptor and donor pinacols. *Journal of the American Chemical Society*, *120*, 439–440.

8. Eck, V., & Holzwarth, J. F. (1982). Fast dynamic phenomena in vesicles of phospholipids. In K. L. Mittal & B. Lindman (Eds.), *Surfactants in solution*, *Vol. 3* (pp. 2059–2080). New York: Plenum.

9. Ganti, T. (1997). Biogenesis itself. *Journal of Theoretical Biology*, *187*, 583–593.

10. Giese, B., Amaudrut, J., Kohler, A., Spormann, M., & Wessely, S. (2001). Direct observation of hole transfer through DNA by hopping between adenine bases and by tunneling. *Nature*, *412*, 318–320.

11. Giese, B. (2002). Long-distance electron transfer through DNA. *Annual Review of Biochemistry*, *71*, 51–70.

12. Gould, I. R., & Farid, S. (1996). Dynamics of bimolecular photoinduced electron-transfer reactions. *Accounts of Chemical Research*, *29*, 522–528.

13. Gust, D., Moore, T. A., & Moore, A. L. (2001). Mimicking photosynthetic solar energy transduction. *Accounts of Chemical Research*, *34*, 40–48.

14. Henderson, P. T., Jones, D., Hampikian, G., Khan, Y., & Schuster, G. B. (1999). Long-distance charge transport in duplex DNA: The phonon-assisted polaron-like hopping mechanism. *Proceedings of the National Academy of Sciences of the U.S.A.*, *96*, 8353–8358.

15. Meggers, E., Dussy, A., Schfer, T., & Giese, B. (2000). Electron transfer in DNA from guanine and 8-oxoguanine to a radical cation of the carbohydrate backbone. *Chemistry—A European Journal*, *6*, 485–492.

16. Munteanu, A., Attolini, C. S.-O., Rasmussen, S., Ziock, H., & Sole, R. (in press). Generic Darwinian selection in protocell assemblies. *Philosophical Transactions of the Royal Society of London, Series B.*

17. Ohashi, M., Otani, S., & Kyushin, S. (1991). Fragmentation of benzyl-esters with an electron-withdrawing group by photoinduced electron-transfer—Analogy with fragmentation in secondary ion mass-spectrometry. *Chemistry Letters*, 631–634.

18. Perrier, S., Sankararaman, S., & Kochi, J. K. (1993). Photoinduced electron-transfer in pinacol cleavage with quinones via highly labile cation radicals—Direct comparison of charge-transfer excitation and photosensitization. *Perkin Transactions*, *2*, 825–837.

19. Rasmussen, S., Chen, L., Deamer, D., Krakauer, D., Packard, N., Stadler, P., & Bedau, M. (2004). Transitions from nonliving to living matter. *Science*, *303*, 963–965.

20. Rasmussen, S., Chen, L., Nilsson, M., & Abe, S. (2003). Bridging nonliving and living matter. *Artificial Life*, *9*, 269–316.

21. Ravanat, J., Saint-Pierre, C., & Cadet, J. (2003). One-electron oxidation of the guanine moiety of 2-deoxyguanosine: Influence of 8-oxo-7,8-dihydro-2-deoxyguanosine. *Journal of the American Chemical Society*, *125*, 2030–2031.

22. Rocheleau, T., Rasmussen, S., Nielsen, P., Jacobi, M., & Ziock, H. (in press). Emergence of protocellular growth laws. *Philosophical Transactions of the Royal Society of London, Series B.*

23. Sakata, Y., Tsue, H., ONeil, M. P., Wiederrecht, G. P., & Wasielewski, M. R. (1994). Effect of donor-acceptor orientation on ultrafast photoinduced electron transfer and dark charge recombination in porphyrin-quinone molecules. *Journal of the American Chemical Society*, *116*, 6904–6909.

24. Sundararajan, C., & Falvey, D. E. (2005). Photorelease of carboxylic acids, amino acids, and phosphates from *N*-alkylpicolinium esters using photosensitization by high wavelength laser dyes. *Journal of the American Chemical Society*, *127*, 8000–8001.

25. Sykora, M., Maxwell, K. A., DeSimone, J. M., & Meyer, T. J. (2000). Mimicking the antenna-electron transfer properties of photosynthesis. *Proceedings of the National Academy of Sciences of the U.S.A.*, *97*, 7687–7691.

26. Szostak, J., Bartel, D., & Luisi, P. L. (2001). Synthesizing life. *Nature*, *409*, 387–390.

27. Whitten, D. G., Chesta, C., Ci, X., & Kellett, M. A. (1991). *Photochemical processes in organized molecular system*. Amsterdam: Elsevier Science Publishers.

28. Zhang, X., Hong, S., Freccero, M., & Mariano, P. S. (1994). Dynamics of α-CH deprotonation and α-desilylation reactions of tertiary amine cation radicals. *Journal of the American Chemical Society*, *116*, 4211–4220.

Appendix

The kinetics of the full reaction scheme is rather complex, so we contract the reaction scheme so that analytical equations for the formation of metabolic products (lipids and oligomers) may be obtained. To accomplish this contraction, two different methods are used. The first involves obtaining a single rate constant for a two-step reaction. Reaction scheme 1 is given by

$$\mathrm{A} \xrightarrow{k_1} \mathrm{B} \xrightarrow{k_2} \mathrm{C}, \tag{16}$$

where A, B, and C are the chemicals of interest, and k_1 and k_2 are the reaction rate constants. The rate of change of [C] may be approximated in terms of [A] only:

$$\frac{d[\mathrm{C}]}{dt} \approx \frac{k_1 k_2}{k_1 + k_2}[\mathrm{A}], \tag{17}$$

which may be simplified if k_1 and k_2 differ greatly. For example, if $k_1 \gg k_2$, the term k_2 in the denominator may be neglected. Then both the numerator and the denominator may be divided by k_1, so that the overall rate constant is equal to k_2. Intuitively, this is sensible because we expect the entire process to be controlled by the step with rate constant k_2 when the step with rate constant k_1 is instantaneous. The error associated with this approximation is greatest when k_1 and k_2 are equal. For normalized concentrations ($[\mathrm{A}](t = 0) = 1$), the maximum error in the product concentration is 0.13. However, the time scales for the completion of the reaction for the full solution and the approximation agree well.

Reaction scheme 2 has the following reaction diagram:

$$\mathrm{A} \underset{k_{m1}}{\overset{k_1}{\rightleftharpoons}} \mathrm{B} \xrightarrow{k_2} \mathrm{C}. \tag{18}$$

In this case, B may undergo back reaction to re-form A with rate constant k_{m1}. For this case, the rate of change of [C] is approximated by

$$\frac{d[\mathrm{C}]}{dt} \approx \frac{k_1 k_2}{k_1 + k_{m1} + k_2}[\mathrm{A}]. \tag{19}$$

This expression may be simplified in the same manner as Equation 17 when values of the rate constants differ significantly. The error associated with this approximation is maximized when k_1 and k_2 are nearly equal and the reverse reaction rate constant k_{m1} is greater than the forward rate constants. For this case, the approximation is essentially identical to reaction scheme 1.